Monthly Notices
of the
ROYAL ASTRONOMICAL SOCIETY

MNRAS **437,** 1808–1820 (2014) doi:10.1093/mnras/stt2009
Advance Access publication 2013 November 13

Periodicity in Class II methanol masers in high-mass star-forming regions

S. Goedhart,[1,2,3]★ J. P. Maswanganye,[2,3] M. J. Gaylard[2] and D. J. van der Walt[3]

[1]*SKA SA, 3rd Floor, The Park, Park Rd, Pinelands, 7405, South Africa*
[2]*Hartebeesthoek Radio Astronomy Observatory, PO Box 443, Krugersdorp, 1740, South Africa*
[3]*School of Physics, North-West University, Potchefstroom campus, Private Bag X6001, Potchefstroom, 2520, South Africa*

Accepted 2013 October 17. Received 2013 October 14; in original form 2013 August 27

ABSTRACT

We report the results of 10 years of monitoring of six regularly varying 6.7 GHz methanol masers using the Hartebeesthoek 26-m telescope. Observations were done at intervals of 1–2 weeks, with faster sampling during flaring episodes. Four of the sources were also monitored at 12.2 GHz and show correlated variations. We find the Lomb–Scargle periodogram to be the most sensitive method to search for periodicity but possibly prone to false detections. Periods range from 132.8 d (with 26 cycles observed) to 509 d (with seven cycles observed). Five of the sources show arguably periodic variations, while G331.13−0.24 shows strong periodicity in one peak, with large and variable delays in other peaks.

Key words: masers – stars: formation – ISM: clouds – H II regions – Radio lines: ISM.

1 INTRODUCTION

Class II methanol masers are well established as tracers of an early stage of massive star formation (Ellingsen 2006, and references therein). The most prevalent and strongest methanol maser line is the $5_1 - 6_0A^+$ transition at 6.7 GHz, first discovered by Menten (1991). To date, over 1000 6.7 GHz methanol masers are known (Pestalozzi, Minier & Booth 2005; Green et al. 2009). The $2_0 - 3_{-1}E$ transition at 12.2 GHz is not as common or as intense but is generally closely associated with the 6.7 GHz masers (Breen et al. 2011). Breen et al. (2011) speculate that sources that have both 6.7 and 12.2 GHz methanol masers may be slightly more evolved than those with only 6.7 GHz masers. The location of the masers in relation to the newly formed star is still not well understood. High-resolution observations have shown masers to have a variety of morphologies (Norris et al. 1993; Phillips et al. 1998; Walsh et al. 1998; Minier, Booth & Conway 2002; Dodson, Ojha & Ellingsen 2004), including linear and curved structures and even a perfect ring shape (Bartkiewicz, Szymczak & Langevelde 2005). Some of these structures have been explained as parts of edge-on or inclined discs (Norris et al. 1993; Minier, Booth & Conway 2000; Pestalozzi et al. 2004), in outflows (Minier et al. 2000) or associated with shocks (Walsh et al. 1998; Dodson et al. 2004).

The high intensity of the methanol masers enables them to be easily monitored with smaller radio-telescope dishes, which typically have more time available for long-term monitoring programmes. Masers are expected to be extremely sensitive to changes in their environment, including local conditions in the volume of masing gas (which may affect the maser path length), as well as the radiation field. Class II methanol masers are believed to be pumped by infrared radiation from warm dust (Sobolev, Cragg & Godfrey 1997; Cragg, Sobolev & Godrey 2002; Cragg, Sobolev & Godfrey 2005) and the masers amplify the continuum emission from background H II regions. Thus monitoring flux density variations in masers could lead to new insights into massive star formation but interpretation of the variation is complicated by the dependence of the maser intensity on many external factors.

Variability in Class II methanol masers was first identified by Caswell, Vaile & Ellingsen (1995). Goedhart, Gaylard & van der Walt (2004) conducted an extensive monitoring program for four years finding several sources that exhibited periodic or quasi-periodic variations. The source G9.62+0.20E was the first confirmed periodic maser (Goedhart, Gaylard & Walt 2003) exhibiting simultaneous flares at 6.7, 12.2 and 107 GHz (van der Walt, Goedhart & Gaylard 2009). The source G12.89+0.49 was found to exhibit rapid variations with a period of 29.5 d. Over 100 cycles were observed in the Hartebeesthoek monitoring program and the data for this source were published separately (Goedhart et al. 2009). To date, only two other periodically variable sources have been detected: IRAS 18566+0408, which also shows correlated variability in a formaldehyde maser with a period of 237 d (Araya et al. 2010), and G22.357+0.066, which has a period of 179 d (Szymczak et al. 2011).

The range of periods found (between 29.5 and 509 d) is inconsistent with stellar pulsations of main-sequence stars, for which periods range between a few hours and 3 d at the most (Moffat 2012). Likewise, stellar rotation rates for massive protostars range from a few days up to 16 d (Nordhagen et al. 2006). Recently, Inayoshi et al. (2013) proposed that periods in the observed range could be explained by pulsation of massive protostars undergoing rapid mass accretion. However, their model does not explain the asymmetric

★E-mail: sharmila@ska.ac.za

Table 1. Observing parameters. Average system temperatures and rms noise are given.

Observation dates	BW (MHz)	Chan.	Vel. res (km s^{-1})	T_{sys} (K)	rms (Jy)
Rest frequency: 6.668518 GHz					
1999/01/17–2003/04/03	0.64	256	0.112	51	0.5
	0.32	256	0.056	51	0.5
2003/07/04–2008/09/30	1.00	1024	0.044	70	0.4
Rest frequency: 12.178593 GHz					
2000/01/30–2003/04/07	0.64	256	0.062	139	2.0
2003/08/25–2008/08/06	1.00	1024	0.048	99	0.3

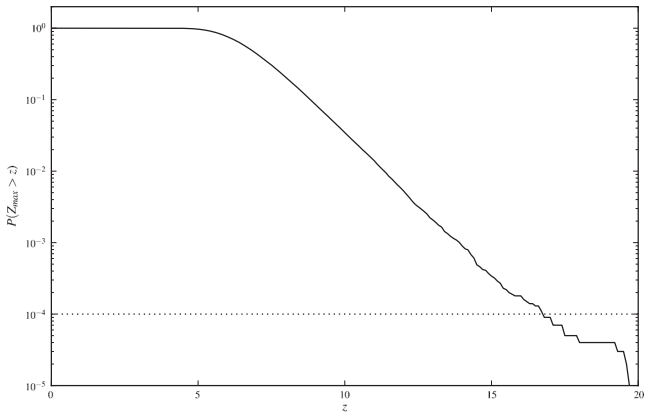

Figure 1. The CDF for the maximum power found for periodograms of synthetic noise for G9.62+0.20 at 6.7 GHz.

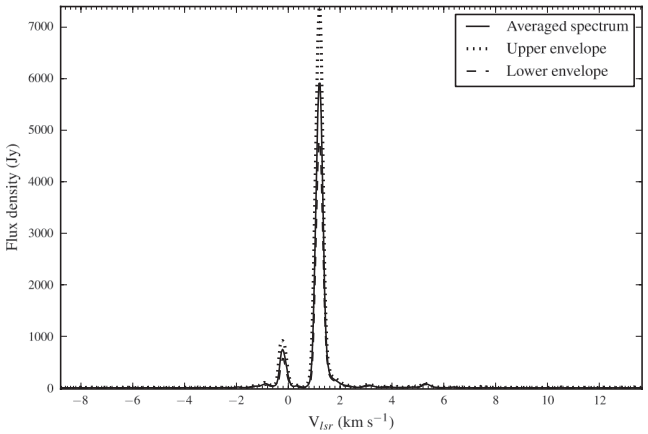

Figure 2. Range of variation across all spectral channels for G9.62+0.19E at 6.7 GHz during 2003–2008.

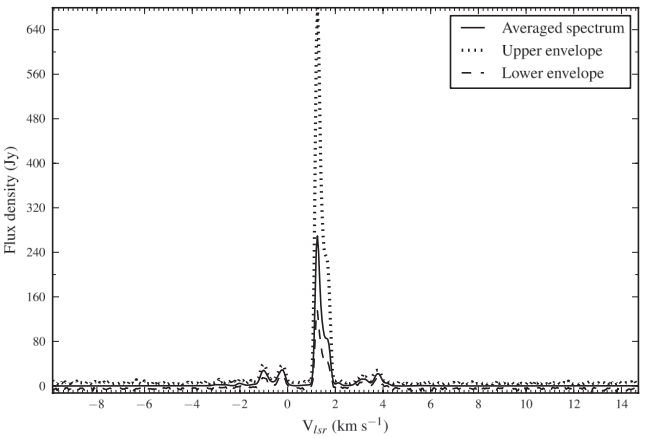

Figure 3. Range of variation across all spectral channels for G9.62+0.19E at 12.2 GHz during 2003–2008.

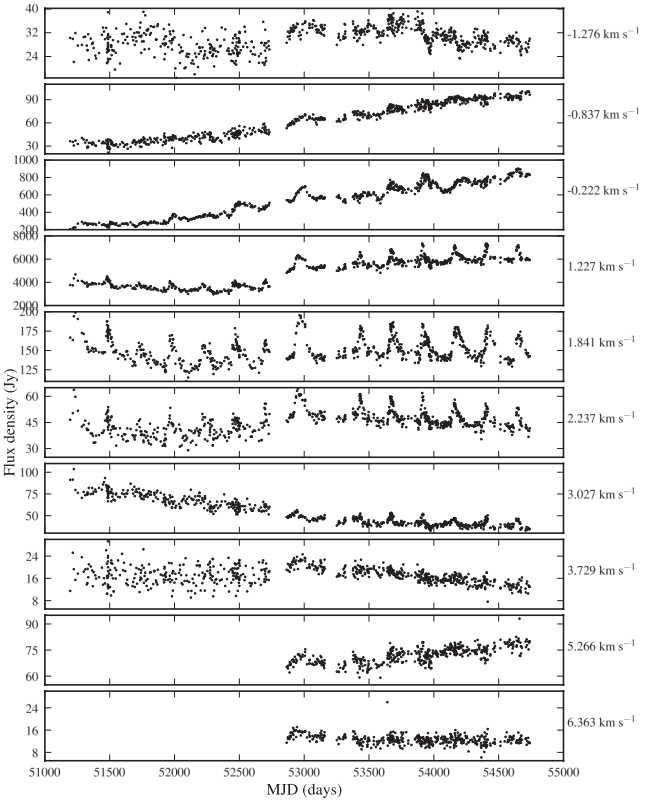

Figure 4. 6.7 GHz time series for peak velocity channels in G9.62+0.19E.

flare profiles seen in several of the masers. On the other hand, binary systems could also explain the range of periods detected. A large fraction (69 per cent) of main-sequence binary stars are found in binary systems and this is expected to be a good representation of their properties at birth (Sana et al. 2012). Apai et al. (2007) surveyed the radial velocities of 16 embedded massive stars and found that 20 per cent of their targets were close binaries. There are a number of ways in which a binary system could modulate maser emission. For example, Muzerolle et al. (2013) have detected periodic variations in the infrared luminosity of a young protostar due to pulsed accretion, modulated by a binary companion. On the other hand, van der Walt (2011) suggests that a colliding-wind binary (CWB) system can explain both the range of periods and the flare profiles of most of the masers. In the CWB model, the maser flares are due to changes in the background free–free emission caused by a pulse of ionizing radiation passing through partially ionized gas. The pulse of radiation is produced by shocked gas from stellar winds when the stars are at periastron. This model can explain the rapid rise of maser intensity as well as the slower decay when the hydrogen recombines.

In this paper, we present the results of approximately 10 years of monitoring of six longer-period sources which have been confirmed to be (quasi-)periodic, from the inception of the monitoring

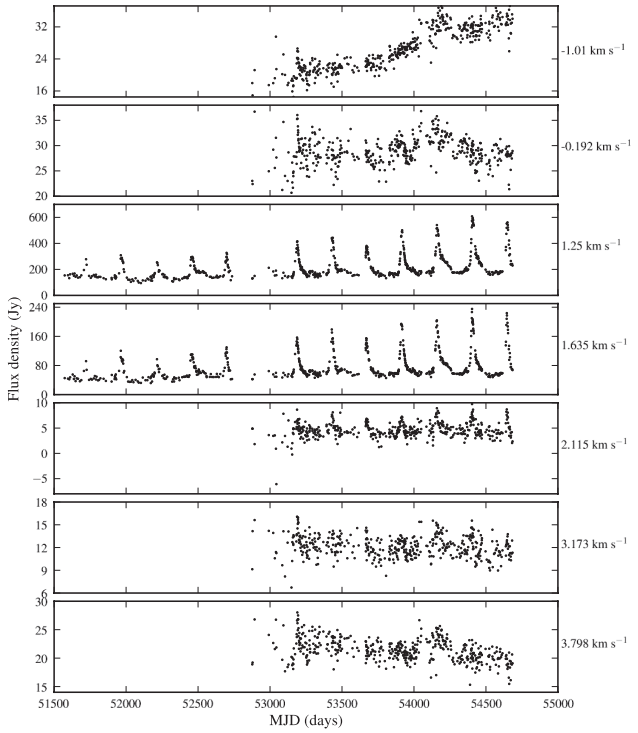

Figure 5. 12.2 GHz time series for peak velocity channels in G9.62+0.19E.

programme up to the failure of the main polar shaft bearing in 2008 October.

2 OBSERVATIONS

All observations were made with the Hartebeesthoek Radio Astronomy Observatory (HartRAO) 26-m telescope. Observing took place at one to two week intervals, with observations at two to three day intervals if a source was seen to be flaring. The antenna surface at this time consisted of perforated aluminium panels. The surface was upgraded to solid panels during 2003–2004, resulting in increased efficiency at higher frequencies. However, the telescope pointing was affected until the telescope was rebalanced in 2005 April and a new pointing model was derived and implemented in 2005 September. Pointing checks during observations were done by observing offset by half a beam-width at the cardinal points and fitting a two-dimensional Gaussian beam model to the observed peak intensities. The sources were observed with hour angle less than 2.3 h to minimize pointing errors. Pointing corrections after the implementation of the new pointing model were typically around 4 to 10 per cent at 12.2 GHz and 1 to 5 per cent at 6.7 GHz. Any observations with pointing corrections greater than 30 per cent were excluded from the final data set since it was found that these were invariably outliers in the time series.

Amplitude calibration was based on regular drift scan measurements of 3C123, 3C218 and Virgo A (which is bright but partly resolved), using the flux scale of Ott et al. (1994). Pointing errors in the north–south direction were measured via drift scans at the beam half power points and the on-source amplitude was corrected using the Gaussian beam model.

During 2003 the receivers were upgraded to dual polarization, and observations were switched to a new control system and a new spectrometer. Frequency-switching mode was used for all observations.

The observing parameters of the monitoring programme are given in Table 1. Prior to 2003 only left circular polarization was recorded and two different bandwidths were used at 6.7 GHz, depending on the target source's velocity range.

The strong methanol maser source G351.42+0.64 was used as a comparison to identify potential periods induced by the telescope systems. No evidence of periodicity was found. Detailed analysis of this source was presented in Goedhart et al. (2009) and will not be repeated in this paper.

Table 2. Periods found from LS periodogram and epoch-folding for G9.62+0.19E. Identified harmonic series are indicated in bold text.

Velocity (km s^{-1})	Mean flux density (Jy)	Mean rms noise (Jy)	S/N	LS Significant periods (d)	E-F period (d)	E-F HWHM (d)
				6.7 GHz		
−1.276	30.1	1.9	15	1575, 945.2, 683.2, 187.8	–	–
−0.837	65.7	2.2	30	1013	–	–
−0.222	564.5	8.4	67	821.9, 443.0, 241.3, 142.1, 131.0	–	–
1.227	5079	75	637	1620, 756.1, 446.5, 268.8, **244.4,127.4, 81.0, 61.0**	243.8	4.1
1.841	151.6	3.4	45	450.1, 272.6, **244.4**, 167.8, 128.0, **121.7, 81.2, 61.0**	243.6	3.8
2.237	45.6	2.1	22	1890, **243.4**, 128.0, **122.0, 81.2, 61.0**	243.7	3.4
3.027	52.0	2.5	23	**246.6**, 225.0, **122.2, 81.7**	242.6	5.5
3.729	17.0	1.9	9	1829	–	–
5.266	72.0	1.4	51	394.7	–	–
6.363	12.6	1.1	11	–	–	–
				12.2 GHz		
−1.010	26.6	0.9	30	1071	–	–
−0.192	28.9	0.9	32	997.5	–	–
1.250	277.5	1.8	124	**244.0, 121.7, 81.1, 60.9, 48.7, 40.6**	243.2	3.6
1.635	79.2	1.3	60	**244.0, 121.7, 81.1, 60.9, 48.7, 40.6**	243.5	2.2
2.115	4.7	0.9	5	**245.2, 120.0, 81.3, 60.6**	243.3	6.5
3.173	12.18	0.9	14	**80.4**	241.6	5.5
3.798	21.5	0.9	24	803.4, 140.4	–	–

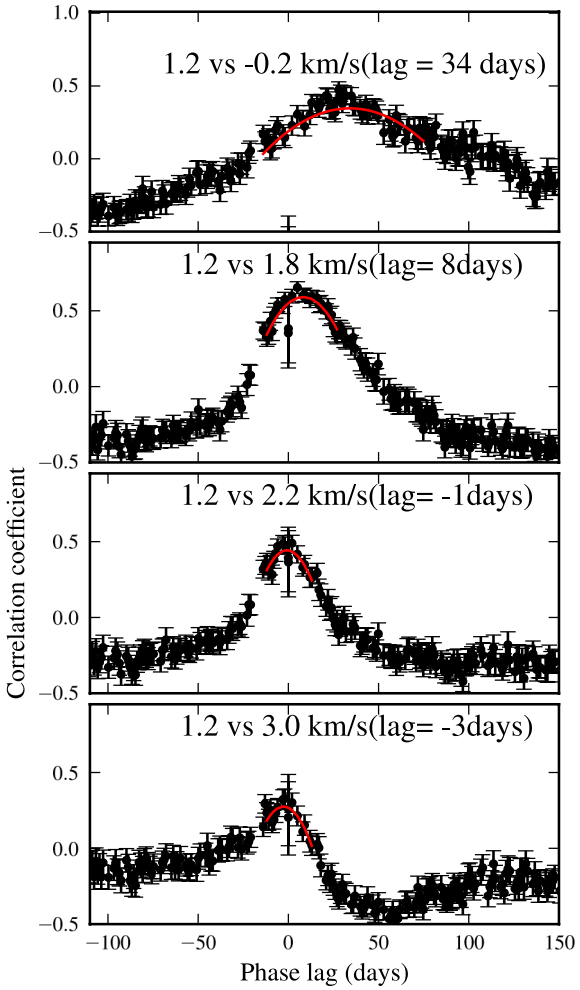

Figure 6. Discrete correlation function between pairs of features at 6.7 GHz for G9.62+0.19E.

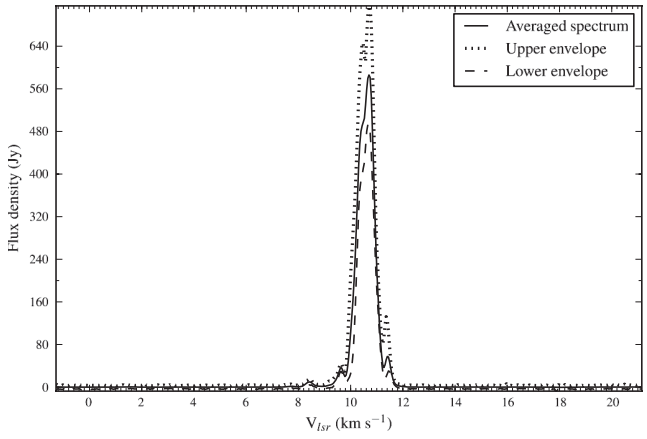

Figure 7. Range of variation across all spectral channels for G188.95 at 6.7 GHz during 2003–2008.

3 PERIOD SEARCH METHODS

There are many methods of searching for periodicities in unevenly sampled astronomical data, most of which are variations on Fourier transforms (e.g. Scargle 1989) or folding data by a trial period and measuring the dispersion of the data points through a test

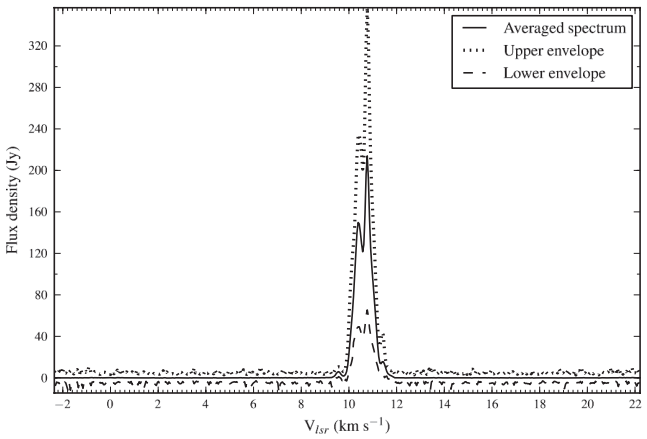

Figure 8. Range of variation across all spectral channels for G188.95+0.89 at 12.2 GHz during 2003–2008.

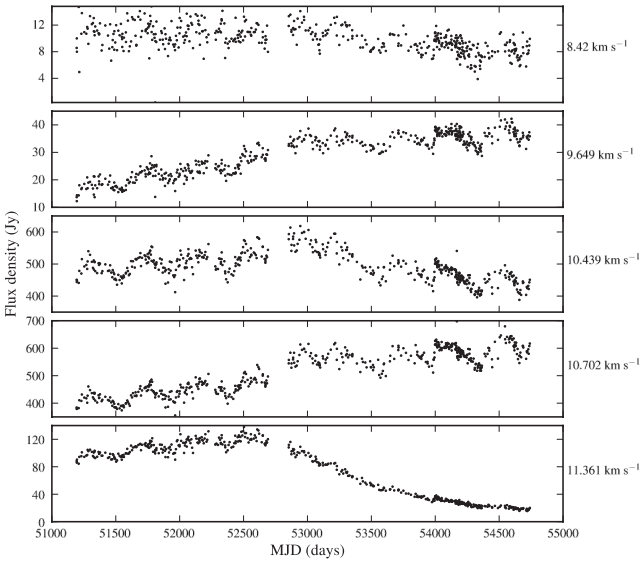

Figure 9. 6.7 GHz time series for peak velocity channels in G188.95+0.89.

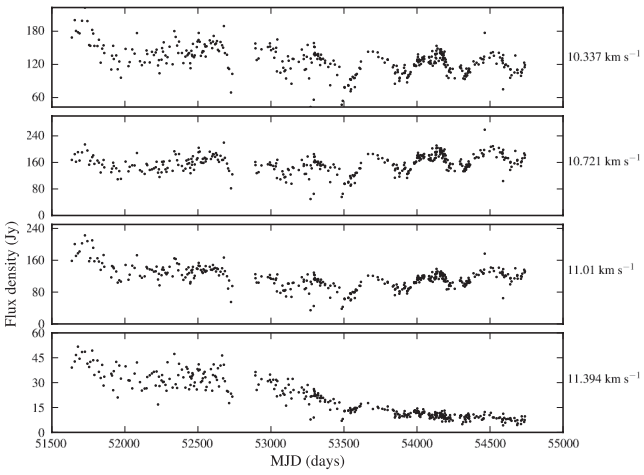

Figure 10. 12.2 GHz time series for peak velocity channels in G188.95+0.89.

Table 3. Periods from LS periodgram and epoch-folding for G188.95+0.89.

Velocity (km s^{-1})	Mean flux density (Jy)	Mean rms noise (Jy)	S/N	LS significant periods (d)	E-F period (d)	E-F HWHM (d)
			6.7 GHz			
8.420	9.8	1.1	9	399.6	393.9	31.0
9.649	29.7	1.7	25	1669, 468.9, 394.0	396.0	16.4
10.439	490.0	9.6	51	1830, 886.4, 472.8, 396.8	393.9	15.8
10.702	520.0	9.5	55	1773.1, 915.2, 472.8, 396.8	396.3	14.5
11.361	71.1	2.1	33	1830, 411.2	399.6, 395.9, 21.8	
			12.2 GHz			
10.337	127.4	1.7	76	1418, 394	–	–
10.721	160.0	1.8	89	1418, 813, 391	–	–
11.010	157.7	1.6	70	1418, 827, 387	–	–
11.394	19.6	1.4	14	1504	–	–

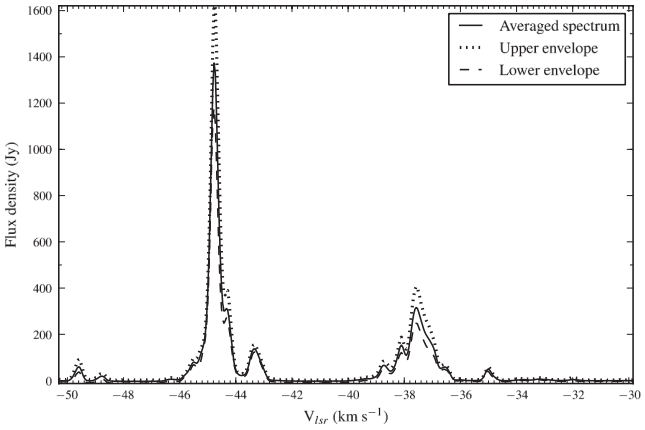

Figure 11. Range of variation across all spectral channels for G328.24−0.55 at 6.7 GHz during 2003–2008.

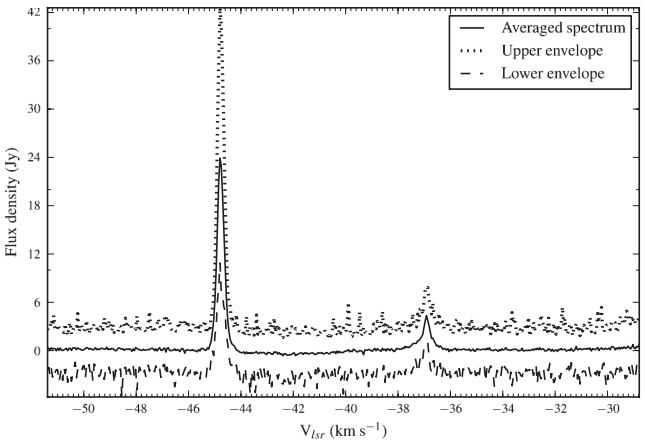

Figure 12. Range of variation across all spectral channels for G328.24−0.55 at 12.2 GHz.

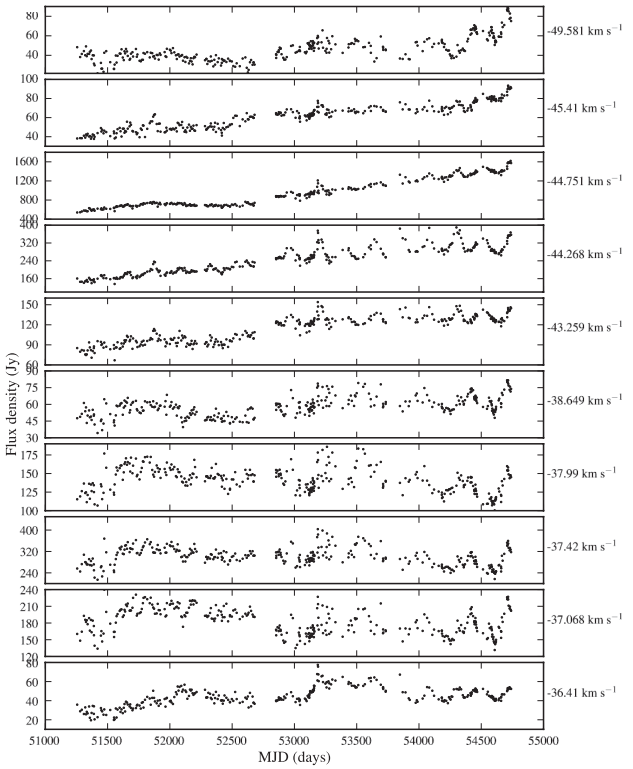

Figure 13. 6.7 GHz time series for peak velocity channels in G328.24−0.55.

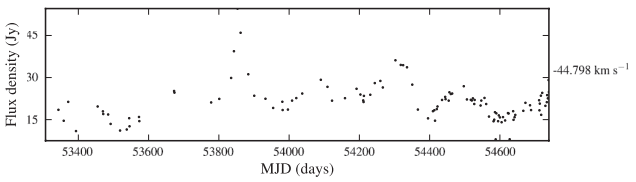

Figure 14. 12.2 GHz time series for the peak velocity channel in G328.24−0.55.

statistic (e.g. Stellingwerf 1978). We have tried a number of different methods of detecting periodicity and found the Lomb–Scargle (LS) periodogram, using the fast algorithm of Press & Rybicki (1989), to be the most sensitive. However, this method can give rise to false detections. We follow the method recommended by Frescura, Engelbrecht & Frank (2008) to determine the false alarm probability function. A cumulative density function (CDF) was constructed from 100 000 Monte Carlo simulations of time series of Gaussian noise, from which the maximum power in the LS periodogram was found. The mean and variance of the noise was estimated from

Table 4. Periods from LS periodogram and epoch-folding for G328.24−0.55.

Velocity (km s^{-1})	Mean flux density (Jy)	Mean rms noise (Jy)	S/N	LS significant periods (d)	E-F period (d)	E-F HWHM (d)
			6.7 GHz			
−49.581	41.3	2.1	20	1548, 311	–	–
−45.410	55.8	2.2	25	1639, 978, 220.3	220.0	5.2
−44.751	805.4	12.4	65	1689, 221.1	221.5	3.5
−44.268	222.0	4.0	55	220.3, 189.6	220.0, 5.7	
−43.259	106.8	2.7	40	1798, 220.3	219.9	5.3
−38.649	56.1	2.2	25	1639, 395, 309.7	–	–
−37.990	145.4	3.3	44	1548.3, 392.5, 352.8, 294.9	–	–
−37.420	308	5.7	55	1506, 389.8, 302.9	–	–
−37.068	185.9	4.0	47	1429, 290.3	–	–
−36.410	43.8	2.1	21	1394, 381.8, 218.6	220.8	8.4
			12.2 GHz			
−44.798	21.2	1.1	20	477.6, 216.3	–	–

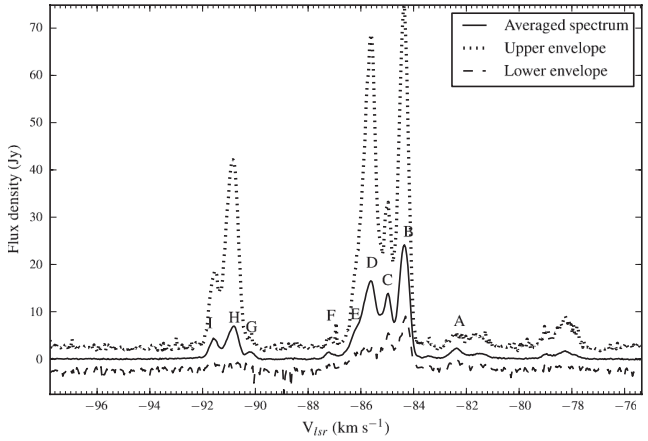

Figure 15. Range of variation across all spectral channels for G331.13−0.24 at 6.7 GHz during 2003–2008.

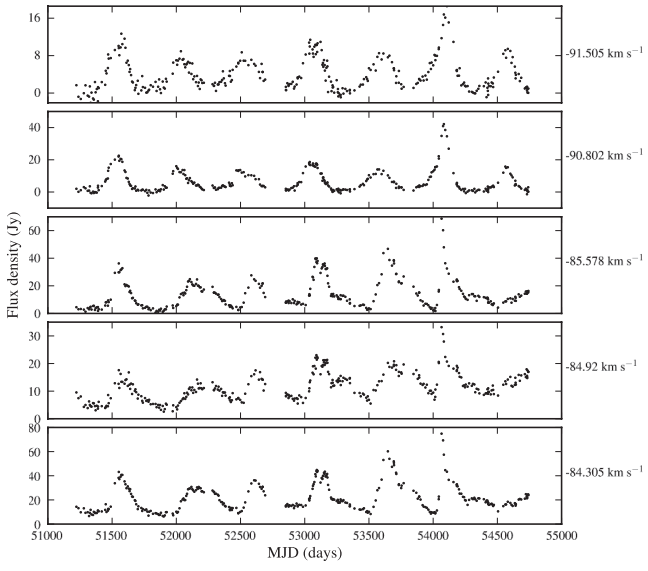

Figure 16. 6.7 GHz time series for peak velocity channels in G331.13−0.24.

emission-free channels in the spectra and the same time-stamps as the observations were used. CDFs were calculated individually for each source and transition. In the cases of G9.62+0.20 and G328.24−0.55 the two observational phases had different noise distributions. This was reflected in the synthetic time series. The effect of oversampling was also investigated, using a conservative factor of 4, and grossly oversampling at a factor of 20. The CDFs are very similar in all cases. Frequencies with false alarm probability $\leq$1e-4 were considered to be significant. Fig. 1 shows the CDF for G9.62+0.20 at 6.7 GHz. We conclude from this that a power level of 16.7 corresponds to a false-alarm probability of 0.01 per cent.

Data were typically detrended using an unconstrained first- or second-order polynomial prior to period search. Despite this, low-frequency components were still found in the data, particularly for some of the maser peaks in G9.62+0.20. Kidger, Takalo & Sillanpaa (1992) discuss the problem of confirming periodicity with the intent to predict future behaviour. They state that the data sample should be of very long duration, covering at least six cycles, and the variations should be of large amplitude. More cycles are necessary to confirm periodicity in the case of objects with low amplitude. This is consistent with our own observations. Goedhart et al. (2004) identified a number of sources which were potentially periodic, but had observed only three cycles for some objects. Continued monitoring of G196.45−1.68 (which had shown two and a half sinusoidal cycles) and G316.64−0.09 (three regularly spaced flares of decreasing amplitude) showed no further evidence of periodic variations.

Epoch-folding was used to verify the frequencies found from the LS periodogram. It was found that the standard epoch-folding method of finding the maximum χ^2 was not very sensitive to flares of varying amplitude. The Davies L-statistic (Davies 1990) appears to be the most sensitive for the sort of time series that we have observed. In the case of sources which may not be strictly periodic, it is useful to have an estimate of the uncertainty in the periods. We investigated methods recommended by Leahy (1987) and Larsson (1996) but these are dependent on being able to accurately model the wave-form of the pulse. Some sources show significant variation in the pulse shape from one cycle to another. All of the sources appear to have varying amplitudes in each cycle, which adds an additional free parameter. The width of the peak in the epoch-folded periodogram appears to be the most robust way to reflect the

Table 5. Periods from LS periodogram and epoch-folding for G331.13−0.24 at 6.7 GHz.

Velocity (km s^{-1})	Mean flux density (Jy)	mean rms noise (Jy)	S/N	LS Significant periods (d)	E-F period (d)	E-F FWHM (d)
−91.505	4.0	0.9	5	507, 370, 255	507.5	19.3
−90.802	6.5	0.9	8	507, 368, 255	507.6	15.8
−85.578	14.3	0.9	16	517, 254	512.8	28.1
−84.920	11.6	0.9	13	816, 503	508.2	27.7
−84.305	22.0	0.9	23	512	511.9	28.5

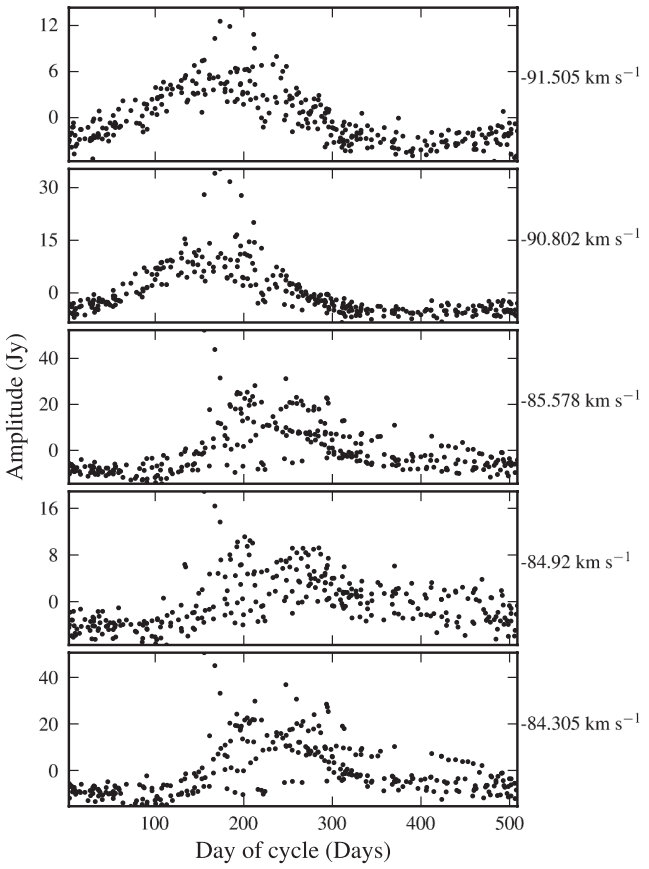

Figure 17. 6.7 GHz time series for G331.13−0.24 folded modulo 510 d. The data have been detrended with a first-order polynomial.

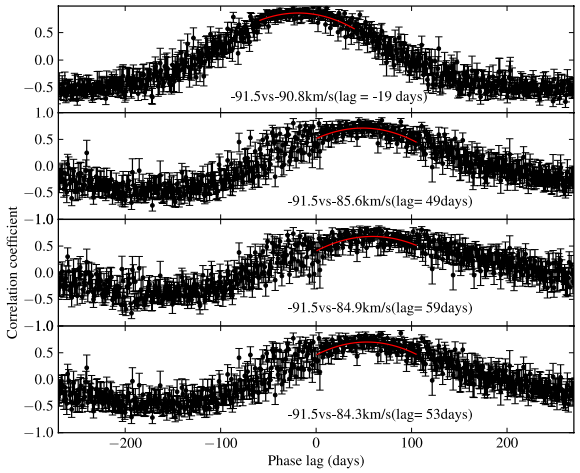

Figure 18. Discrete correlation function between pairs of features for G331.13−0.24.

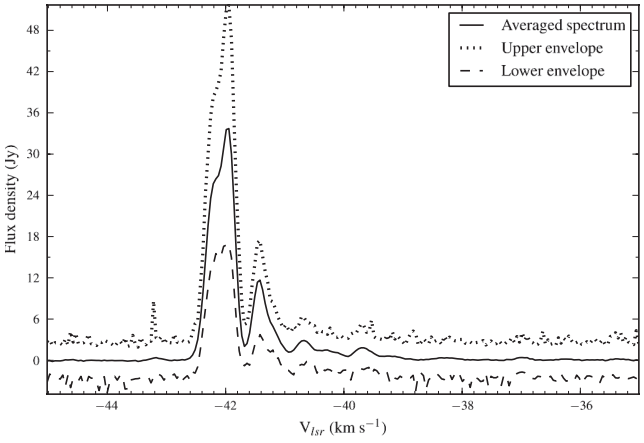

Figure 19. Range of variation across all spectral channels for G338.93−0.06 at 6.7 GHz during 2003–2008.

uncertainty in the periods. In the case of quasi-periodic sources, this is not due to measurement errors, but is a reflection of the spread in times at which the flares peak.

4 RESULTS

The LS periodograms will be available online as supplementary material.

4.1 G9.62+0.19E

G9.62+0.20E is the brightest 6.7 GHz methanol maser known and was observed to reach a peak flux density of 7344 Jy on 2006 June 24. It has been found to be associated with the H II region E in the massive star-forming complex G9.62+0.20 (Garay et al. 1993) and was classified as a hypercompact H II region by Kurtz & Franco (2002). The distance to this region from trigonometrical parallax of the 12.2 GHz masers is 5.2 kpc (Sanna et al. 2009). Infall motions with HCN (4–3) and CS (7–6) lines were found towards the submillitre core in region E with an infall rate of $4.3 \times 10^{-3} M_{\odot}$ yr^{-1} (Liu et al. 2011).

The range of variation for all spectral channels for G9.62+0.19E at 6.7 and 12.2 GHz is shown in Figs 2 and 3. We calculate the maximum, mean and minimum over time for each channel. The

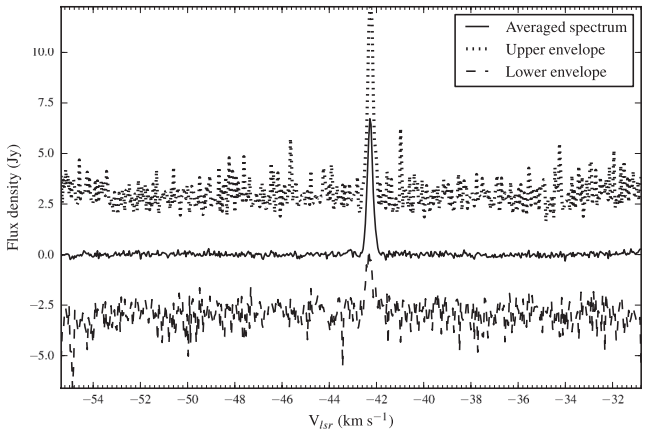

Figure 20. Range of variation across all spectral channels for G338.93−0.06 at 12.2 GHz.

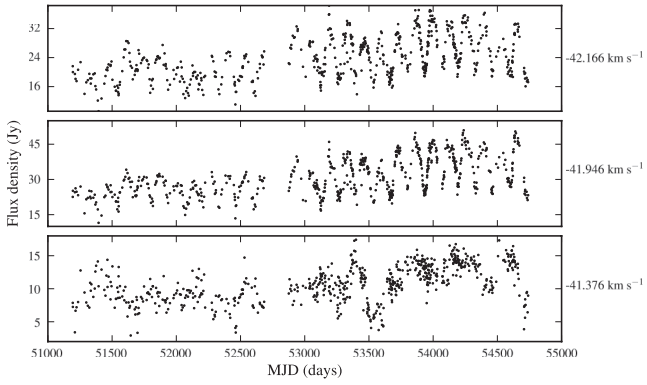

Figure 21. 6.7 GHz time series for peak velocity channels in G338.93−0.06.

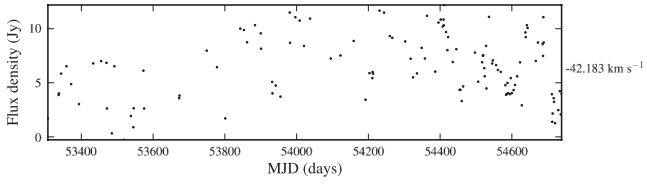

Figure 22. 12.2 GHz time series for the peak velocity channel in G338.93−0.06.

time series for the peak channels at 6.7 GHz is shown in Fig. 4 and at 12.2 GHz in Fig. 5. At 6.7 GHz, the components at −0.837, −0.222, 1.227 and 5.266 km s^{-1} have been steadily increasing in mean intensity, while the components at 3.027 and 3.729 km s^{-1} have been decreasing. The mean brightness of the components at 12.2 GHz has also been increasing slowly but most notable is the increase in the amplitude of the flares in the 1.250 and 1.635 kms s^{-1} components.

Table 2 summarizes the periods found from the LS periodogram and epoch-folding. The time series were detrended using a third-order polynomial. Several low-frequency components were found with high power, corresponding to long-term trends in the data. Following the criteria of Kidger et al. (1992) we consider a period to be confirmed only if at least six cycles have been observed. The period with the highest power, for any of the spectral features at 6.7 GHz, is 244.4 d. Clear periodicity is seen in the features at 1.227, 1.841, 2.237 and 3.027 km s^{-1} . A harmonic series is seen in the periodograms for 1.841 and 2.237 km s^{-1} . At 12.2 GHz the period with the highest power is 244.0 d. Clear periodicity is seen in the same velocity range as for the 6.7 GHz transition and several features show a harmonic series. The large number of significant frequencies found seem unlikely to be real detections. The periods were investigated further using epoch-folding. Clear peaks are only seen for periods corresponding to ∼243 d and multiples thereof. Similar results are seen for the 12.2 GHz data. Taking the weighted mean of the epoch-folded periods we find a period of 243.3 ± 2.1 d. The time series were folded modulo the other periods derived from the LS periodogram but no clear waveform was seen.

Delays in flaring between features were estimated using the z-transformed discrete correlation function of Alexander (1997). We use the 1.227 km s^{-1} feature as the reference. At 6.7 GHz there appears to be a lag of 34 d between the dominant peak and the −0.222 km s^{-1} feature (Fig. 6). There may be an 8 d lag between 1.183 and 1.841 km s^{-1} . There are smaller lags between the main peak and 2.2 and 3.0 km s^{-1} but these may not be significant given the noise in the correlation function. No lags are found between the features in the 12.2 GHz time series and there is no lag between the same velocity features at 12.2 and 6.7 GHz.

4.2 G188.95+0.89

These masers are situated in the star-forming region AFGL 5180 or S252. VLBI observations at 6.7 and 12.2 GHz show a linear distribution, with the two transitions spatially co-located (Minier et al. 2000). No continuum radio source has been detected, but the masers are projected on a bright mm source with an estimated mass of 50 $m_\odot$ (MM1 in Minier et al. 2005). Longmore et al. (2006) estimate the mass of the mid-infrared core associated with the methanol masers to be 7 $M_\odot$ based on its luminosity of 8.4 $L_\odot$. Parallax measurements of water masers associated with the star-forming region place it at a distance of 2.02 kpc (Niinuma et al. 2011).

Figs 7 and 8 show the range of variation in the spectra at 6.7 and 12.2 GHz, respectively. The time series are shown in Figs 9 and 10. As with G9.62+0.20, the variations are much more pronounced at 12.2 GHz. The first five cycles at 6.7 GHz show a sinusoidal waveform, but the last four cycles show more of a sawtooth pattern. The feature at 11.361 km s^{-1} has been steadily weakening since early 2004 but weak periodic variations can be seen. van der Walt (2011) explains this decay by recombination of the ionized gas in part of the H II region along the line of sight to this maser.

Two separate polynomials were used to detrend the time series for the feature at 11.3 km s^{-1} prior to period search. The periods above the significance threshold for the LS periodogram and the periods found from epoch-folding are summarized in Table 3. The epoch-fold peaks at 12.2 GHz were asymmetrical and noisy, so they have not been fitted. Using the 6.7 GHz values only we find a weighted mean period of 395 ± 8 d. No phase lags between features were found.

4.3 G328.24−0.55

There are two maser groups in the beam, viz. G328.236−0.547 and G328.254−0.532 (Phillips et al. 1998). G328.236−0.547 is broken up into two groups with velocity ranges −46 to −42 km s^{-1} and −37 to −31 km s^{-1} . G328.254−0.547 has features at −50 km s^{-1} and at −40 to −36 km s^{-1} . The latter group is unfortunately blended with G328.254−0.532 and the spectra are probably

Table 6. Periods from LS periodogram and epoch-folding for G338.93−0.06.

Velocity (km s^{-1})	Mean flux density (Jy)	Mean rms noise (Jy)	S/N	L-S Significant periods (d)	E-F period (d)	E-F FWHM (d)
				6.7 GHz		
−42.166	24.0	0.9	26	1158, 132.6, 87.4, 84.9, 66.4	132.8	1.4
−41.946	31.2	1.0	32	132.6, 66.4	132.9	1.1
−41.376	10.9	0.8	13	2837, 1320, 396.8, 297.1, 235.4, 201.9, 86.8	–	–
				12.2 GHz		
−42.183	6.43	1.0	6	132.4	132.6	4.4

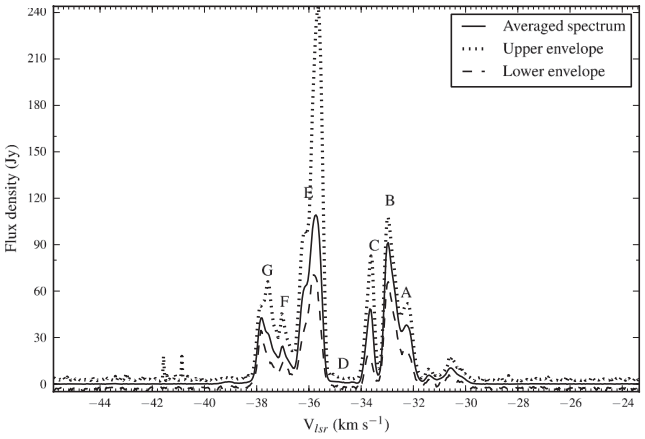

Figure 23. Range of variation across all spectral channels for G339.62−0.12 at 6.7 GHz during 2003–2008.

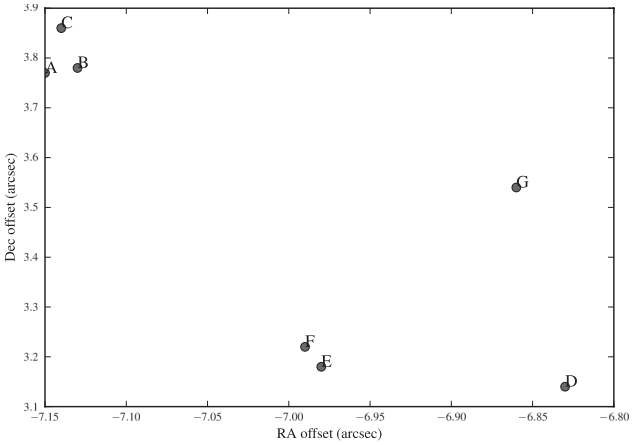

Figure 25. Distribution of maser spots for G339.62−0.12 from table 2 of Walsh et al. (1998).

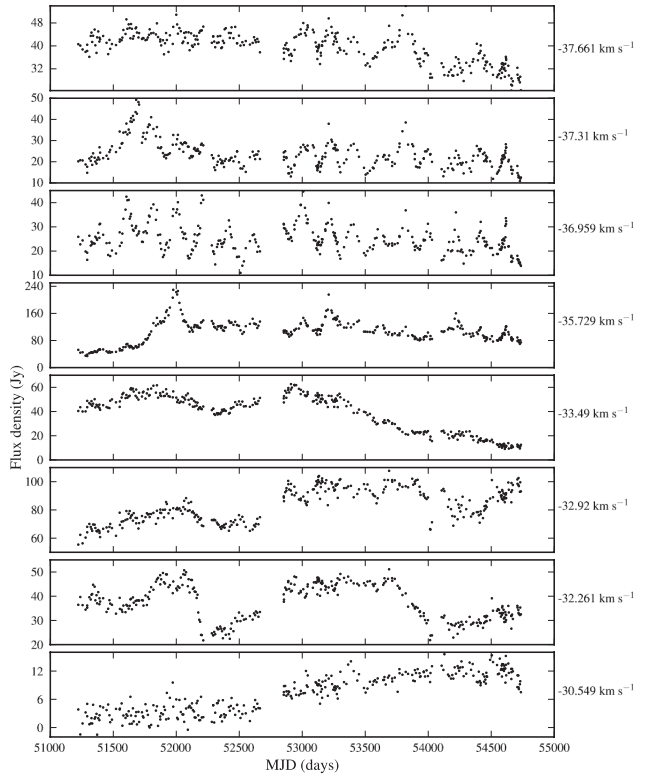

Figure 24. 6.7 GHz time series for peak velocity channels in G339.62−0.12.

dominated by the emission from this group. The two velocity groups in G328.236−0.547 are separated by 83 arcsec and lie on either side of an unresolved H II region. Phillips et al. (1998) offer three explanations for this morphology: shock fronts in a bipolar outflow, two clusters on either side of a thick disc, or two separate sources in a binary system. Dodson et al. (2004) imaged this region with the Australian Long Baseline Array and find that the maser spots may have a linear distribution. However, they find no reason to think that the two regions could be related since there is no alignment in position angle of the maser spots. These regions are estimated to be at the near kinematic distance of 3 kpc.

Figs 11 and 12 show the range of variation in the spectra at 6.7 and 12.2 GHz, respectively. There is only one spectral feature at 12.2 GHz strong enough for analysis. Figs 13 and 14 show the time series. We see correlated periodic variations across several peaks corresponding to the velocity range covered exclusively by G328.236−0.547. The overall intensity of the peak at −44.751 km s^{-1} has increased almost threefold since the start of the monitoring programme. The average intensity of the features corresponding to G328.254−0.532 does not show the same trend. The 6.7 GHz periodograms are dominated by long-term trends. Epoch-folding after a second-order detrend finds a weighted mean period of 220.5 ± 1.0 d for five features: −45.410, −44.751, −44.268, −43.259 and −36.410 km s^{-1}. The significant periods found in the LS periodogram and best-fitting periods from epoch-folding are summarized in Table 4. The highest spectral power is found for a period of 220.3 d. The 12.2 GHz epoch-folded periodogram is not as sharply delineated as at 6.7 GHz because of the shorter time

Table 7. Periods from LS periodogram and epoch-folding for G339.62−0.12 at 6.7 GHz.

Velocity (km s^{-1})	Mean flux density (Jy)	Mean rms noise (Jy)	S/N	LS Significant periods (d)	E-F period (d)	E-F HWHM (d)
−37.661	39.3	1.2	32	685.5, 201	200.9	6.5
−37.310	23.4	1.1	22	1606, 1222, 892, 703, 557, 199	198.7	4.6
−36.959	25.1	1.1	23	1249, 200	200.6	2.7
−35.729	106.4	2.0	54	2677, 1196, 446, 201	200.7	8.5
−33.490	38.4	1.3	31	1479	–	–
−32.920	83.4	1.7	50	1653, 936, 202	201.0, 5.1	
−32.261	37.3	1.2	31	1653, 892	–	–
−30.549	7.3	1.0	7	2555	–	–

Table 8. Summary of periods and the observation statistics.

Source (transition)	Period (d)	σP (d)	Num. obs	Time-span (d)	Num. cycles
G9.62+0.19E (6.7 GHz)	243.3	2.1	708	3544	14.5
G9.62+0.19E (12.2 GHz)			617	3111	12.7
G188.95+0.89 (6.7 GHz)	395	8	488	3544	9.1
G188.95+0.89 (12.2 GHz)			373	3102	7.9
G328.24−0.55 (6.7 GHz)	220.5	1.0	320	3483	15.8
G328.24−0.55 (12.2 GHz)			112	1432	6.5
G331.13−0.24 (6.7 GHz)	509	10	318	3519	6.9
G338.93−0.06 (6.7 GHz)	132.8	0.8	653	3544	26.7
G338.93−0.06 (12.2 GHz)			123	1431	10.7
G339.62−0.12 (6.7 GHz)	200.3	1.1	315	3513	17.5

series. We adopt a weighted mean period of 220.5 ± 1.0 d. The changing amplitudes of the flares leave the peaks weakly defined. The features corresponding to G328.254−0.547 show correlated, regular variations with a characteristic period close to 300 d but the epoch-fold does not show peaks corresponding to those found by the LS periodogram and no clear waveform is seen when the time series are folded modulo 300 d. The variations show no correlation with G328.236−0.547. No time-delays were found.

4.4 G331.13−0.24

The maser spots in this source have a linear distribution with a velocity gradient, except for a single component (Phillips et al. 1998). The masers lie at the edge of an extended H II region with an irregular morphology. Phillips et al. (1998) speculate that there may be more than one star embedded in the UC H II region because the masers are offset from the centre. De Buizer et al. (2009) included this region in their sample to search for outflows associated with linear maser structures. Using ATCA, they find SiO emission centred on the maser location and distributed at a very similar angle to the masers although the outflow may be oriented along the line of sight. There is a 3 mm continuum source which overlaps with the cm continuum source but is slightly offset.

Fig. 15 shows the spectra at 6.7 GHz with the spots mapped by Phillips et al. (1998) indicated. While there are 12.2 GHz masers associated with this source, they lie below the detection threshold of the 26-m telescope. The 6.7 GHz time series are plotted in Fig. 16. All peaks show repeated flares with a delay between the two velocity groupings. The last flare failed to manifest at the expected time in the second grouping. The second grouping is also showing a gradual increase in the base level intensity. The LS periodograms show a spread in periods of about 7 d (Table 5). The spread in derived periods may be due to the flares not repeating very well. The epoch-folded peaks are correspondingly very broad. We adopt a weighted mean period of 509 ± 10 d from the epoch-folded periodograms. In Fig. 17 we show the time series folded modulo 509 d. The delays between the peak of the flares can be clearly seen. It is also clear that the second group of masers (B, C and D) does not flare as regularly as the first group (H and I). Fig. 18 shows the discrete correlation function between the reference feature at −91.505 km s^{-1} (spot I) and the other features. The magnitude of the delay is estimated by fitting a second-order polynomial to the peak of the correlation function but the peaks are quite broad and the derived delays should be treated with care. The changing pulse shapes make it very difficult to identify the exact magnitude of the delay. The feature at H starts to flare at the same time as I, but it appears to peak about 19 d earlier. Feature D flares about 49 d after I, and features C and B flare 59 and 53 d later. Broadly outlined, this implies that the flare propagates from the south-west (closer to the peak of the H II region) to the north-east. The resolution of the SiO maps from ATCA is unfortunately not good enough to determine if the flaring is related to the outflow. We would also need to be able to know the absolute positions of the masers relative to the outflow.

4.5 G338.93−0.06

This source does not appear to have been mapped at cm wavelengths.

Figs 19 and 20 show the spectra at 6.7 and 12.2 GHz. The time series at 6.7 and 12.2 GHz are shown in Figs 21 and 22. Two of the peaks at 6.7 GHz show correlated periodic variability. The third peak at −41.376 shows variability and also shows significant power in the LS periodogram. The periods found are summarized in Table 6. The 12.2 GHz peak shows the same periodicity as the 6.7 GHz peaks at −42.166 and −41.946 km s^{-1} but is not as well sampled as at 6.7 GHz. The epoch-folded periodograms also indicate a remarkable level of periodicity. We derive a weighted mean period using the longer time series at 6.7 GHz of 132.8 ± 0.8 d. The wave form of this source is different from the other periodic sources since it shows a very sharply defined minimum and does not have a quiescent period. No discernable delays were found between the two periodic features.

4.6 G339.62−0.12

The 6.7 GHz spectra are shown in Fig. 23 with maser features mapped by Walsh et al. (1998) indicated. The time series for the peak velocity channels is shown in Fig. 24. The features at −37.661, −37.310, −36.959 and −32.92 km s^{-1} show correlated periodic variations. We plotted the maser spots listed in table 2 of Walsh et al.

(1998) in Fig. 25 since it is necessary to understand the variability of the different features. The feature at $-30.549\,\mathrm{km\,s^{-1}}$ was not detected by Walsh et al. (1998) but has been steadily increasing in intensity. Table 7 summarizes the peaks in the LS and epoch-folding periodograms. Each individual feature shows its own uncorrelated variability, in addition to the shared periodic flares. Spots A, B and C form a tight cluster to the north-east of the region and spot D seems to have vanished. Spots E, F and G are slightly dispersed but all show a common periodicity. The same periodicity is probably also present in spot B. We adopt a weighted-mean period of 200.3 ± 1.1 d. The uncorrelated variability as well as the destruction and formation of new maser spots seems to point to volatile local conditions. No discernable delays were found.

5 DISCUSSION

We summarize the confirmed periods in Table 8, including the number of observations, the time-span covered and the number of cycles observed. The observations cover a sufficiently long time-span to confirm true periodicity in these sources. The range of periods observed (including the 29.5 d period reported for G12.89+0.49) can only be readily explained by orbital motions, most probably due to a binary system.

Fig. 26 shows a comparative diagram of the normalized folded wave forms for a representative feature from each source. The normalized fold was produced by dividing the time series into cycles based on its best-fitting period, and the flux density measurements in each cycle were divided by the maximum recorded in the cycle. The time-axis was normalized by dividing by the period. Some generalizations can be made regarding the waveforms. G9.62+0.20, G328.24−0.55 and G339.62−0.12 show sharply peaked asymmetric pulse profiles, while G188.95+0.89 is closer to sinusoidal. The simple CWB model of van der Walt (2011) is able to reproduce these waveforms by modification of the orbital parameters of the binary system.

The behaviour of G338.93−0.06, on the other hand, with very sharply defined minima and no quiescent phase, cannot be explained by the CWB model. In the model, changes in the free–free emission amplified by the maser is due to a combination of the orbital motion of the secondary star and the partial recombination of the ionized gas at the ionization front. The peak of the maser flare corresponds to periastron passage while the minimum corresponds to apastron. Under the assumption of the adiabatic cooling of the shocked gas, the luminosity of shocked gas varies as $1/r$ where r is the distance between the two stars. The luminosity and therefore the flux of ionizing photons increase rapidly as periastron is approached followed by a slower decay due to the recombination of the partially ionized gas in the ionization front for a rather eccentric orbit. This explains the asymmetric flare profile of some of the maser sources such as seen in, for example, G9.62+0.20E. However, the $1/r$ dependence will always result in a rather slow increase of the flux of ionizing photons just after apastron. It is therefore difficult to explain the sharp increase in the maser flux density as in the case of G338.93−0.06 within the framework of the CWB model.

G331.13−0.24 with its changes in pulse profile between cycles and features is also not consistent with a simple CWB model. We note that G12.89+0.49, while having the shortest period known, also has similar characteristics to G331.13−0.24, with a very stable phase for the minima of the light curve but varying phase for the peak. G331.13−0.24 is the only source in this sample associated with a known outflow. It is possible that the methanol masers, while not directly associated with the outflow, could be amplifying emission from an episodic or precessing outflow. One of the mechanisms put forward by MacLeod & Gaylard (1996) for strong phase lags in methanol maser flares in G351.78−0.54 was an intermittent thermal jet. A strong bipolar outflow has subsequently been found towards this source (Leurini et al. 2009).

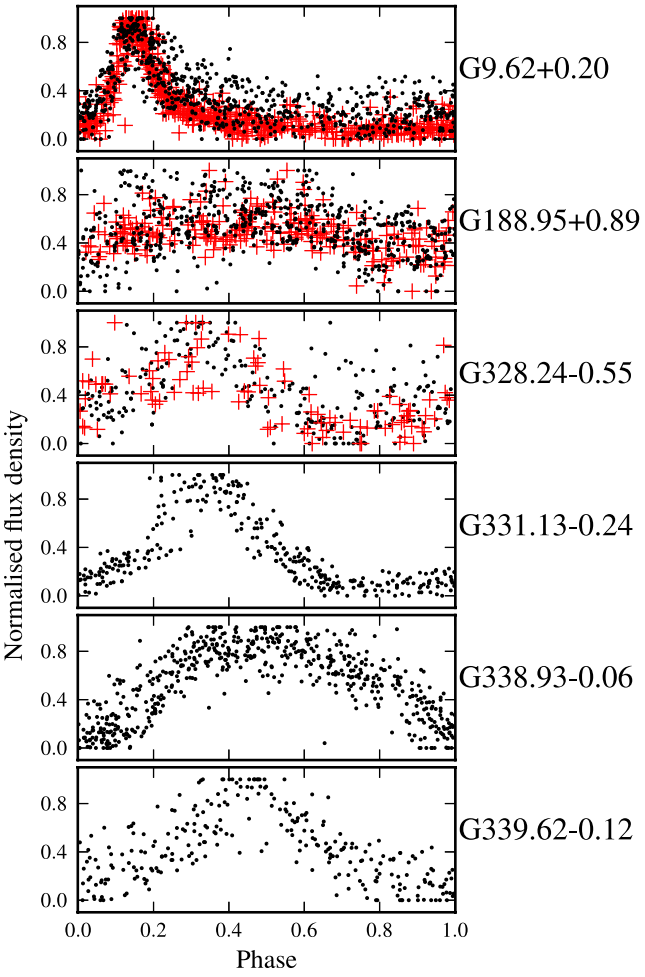

Figure 26. Normalized folded waveforms for each periodic source. The dots are for 6.7 GHz measurements and the crosses are for 12.2 GHz, where available.

There is also a very close correspondence between 12.2 and 6.7 GHz waveforms, where we are able to achieve sufficient signal-to-noise ratio, indicating a common mechanism. van der Walt et al. (2009) have also observed simultaneous flaring at 107 GHz for G9.62+0.19E. The 12.2 GHz masers show higher amplitude variations, in general.

The periods appear to be stable for all of the sources. The spectral structure of the sources also appears to be stable in general, although some features may slowly change in intensity over time. The masers tend to return to a similar intensity after a flare, indicating that the maser region itself is not affected by the mechanism causing the periodic modulation. This was confirmed by high-resolution observations of G9.62+0.20E during a flare (Goedhart et al. 2005). However, the varying amplitudes of flares and long-term trends may be due to local changes in maser path length.

It may be significant that all of these sources have both 6.7 and 12.2 GHz methanol masers, even if they may not be strong enough for monitoring with the 26-m telescope. All of the sources, with the exception of G188.95+0.89, appear to have OH maser

emission as well. The statistical analysis of Breen et al. (2011) indicates that these objects are at a more advanced evolutionary stage than those exhibiting only 6.7 GHz maser emission. Most of the periodic sources, with the exception of G188.95+0.89 and possibly G339.62−0.12, have been getting brighter.

Understanding the underlying mechanism of these periodic variations is limited by observational constraints. Monitoring of the flux density of the associated H II regions is challenging due to confusion and the variable uv-coverage of interferometric arrays. However, monitoring of other maser species may enable us to constrain whether the variability lies with the seed or pump photons. Mainline-hydroxyl masers are believed to have a common pump mechanism with Class II methanol masers and simultaneous monitoring of methanol and hydroxyl masers will be valuable. Green & Caswell (2012) looked for variations in the OH maser in G12.89+0.89 and found an indication that there may be a drop in intensity coinciding with the same effect at 6.7 GHz. A programme to monitor the OH masers using the HartRAO 26 m and the newly commissioned KAT-7 telescope has been started and should give us greater insight into the variability of OH masers associated with periodic methanol sources. Araya et al. (2010) find quasi-periodic variations in the formaldehyde maser in IRAS 18566+0408, with correlated variations in some of the 6.7 GHz methanol maser components. The pump mechanism of formaldehyde is not fully understood – Boland & Jong (1981) show that the masers can be pumped by the free–free continuum radiation from an H II region, while Araya et al. (2010) argue that the simultaneous flaring of methanol and formaldehyde indicate a common infrared pump and that the variability is caused by periodic accretion of circumbinary disc material.

6 CONCLUSIONS

We have presented 10 years of monitoring of six periodic Class II methanol masers. The periods in this sample range from 132.8 to 509 d. The regularity of the flares indicates a periodic underlying mechanism, while the amplitude of the maser response can vary. Where it is possible to monitor the 12.2 GHz methanol masers, these have been found to flare simultaneously with their 6.7 GHz counterparts.

While the cause of the periodicity is yet to be confirmed, it seems likely that these sources are associated with binary systems. Further work needs to be done in developing time-dependent maser pump models and in finding associated variability in other tracers.

ACKNOWLEDGEMENTS

Part of S Goedhart's work on this project has been supported by the National Research Foundation under grant number 74886.

REFERENCES

Alexander T., 1997, in Maoz D., Sternberg A., Leibowitz E. M. eds, Astronomical Time Series. Kluwer, Dordrecht, p. 163
Apai D., Bik A., Kaper L., Henning T., Zinnecker H., 2007, ApJ, 655, 484
Araya E., Hofner P., Goss W. M., Kurtz S., Richards a. M. S., Linz H., Olmi L., Sewiło M., 2010, ApJ, 717, L133
Bartkiewicz A., Szymczak M., Langevelde H. J. V., 2005, A&A, 442, L61
Boland W., Jong T. D., 1981, A&A, 98, 149
Breen S. L., Ellingsen S. P., Caswell J. L., Green J. a., Fuller G. a., Voronkov M. a., Quinn L. J., Avison a., 2011, ApJ, 733, 80
Caswell J. L., Vaile R. A., Ellingsen S. P., 1995, Proc. Astron. Soc. Aust., 12, 37
Cragg D. M., Sobolev A. M., Godrey P. D., 2002, MNRAS, 331, 521
Cragg D. M., Sobolev A. M., Godfrey P. D., 2005, MNRAS, 360, 533
Davies S., 1990, MNRAS, 244, 93
De Buizer J. M., Redman R. O., Longmore S. N., Caswell J., Feldman P. A., 2009, A&A, 493, 127
Dodson R., Ojha R., Ellingsen S. P., 2004, MNRAS, 351, 779
Ellingsen S. P., 2006, ApJ, 638, 241
Frescura F. A. M., Engelbrecht C. A., Frank B. S., 2008, MNRAS, 388, 1693
Garay G., Rodríguez L. F., Moran J. M., Churchwell E., 1993, ApJ, 418, 368
Goedhart S., Gaylard M., Walt D., 2003, MNRAS, 36, L33
Goedhart S., Gaylard M. J., van der Walt D. J., 2004, MNRAS, 355, 553
Goedhart S., Minier V., Gaylard M., van der Walt D. J., 2005, MNRAS, 356, 839
Goedhart S., Langa M. C., Gaylard M. J., van der Walt D. J., 2009, MNRAS, 398, 995
Green J. A., Caswell J. L., 2012, MNRAS, 425, 1504
Green J. A. et al., 2009, MNRAS, 392, 783
Inayoshi K., Sugiyama K., Hosokawa T., Motogi K., Tanaka K. E. I., 2013, ApJ, 769, L20
Kidger M., Takalo L., Sillanpaa A., 1992, A&A, 264, 32
Kurtz S., Franco J., 2002, Rev. Mex. Astron. Astrofis., 12, 16
Larsson S., 1996, A&AS, 117, 197
Leahy D., 1987, A&A, 180, 275
Leurini S., Codella C., Zapata L. A., Belloche A., Stanke T., Wyrowski F., Schilke P., 2009, A&A, 507, 1443
Liu T., Wu Y., Liu S.-Y., Qin S.-L., Su Y.-N., Chen H.-R., Ren Z., 2011, ApJ, 730, 102
Longmore S. N., Burton M. G., Minier V., Walsh A. J., 2006, MNRAS, 369, 1196
MacLeod G., Gaylard M. J., 1996, MNRAS, 280, 868
Menten K. M., 1991, ApJ, 380, L75
Minier V., Booth R. S., Conway J. E., 2000, A&A, 362, 1093
Minier V., Booth R. S., Conway J. E., 2002, A&A, 383, 614
Minier V., Burton M. G., Hill T., Pestalozzi M. R., Purcell C. R., Garay G., Walsh A. J., Longmore S., 2005, A&A, 429, 945
Moffat A. F. J., 2012, in Drissen L., Rubert C., St-Louis N., Moffat A. F. J., eds, ASP Conf. Ser. Vol. 465, Proc. Sci. Meeting in Honor of Anthony F. J. Moffat. Pulsations of Massive Stars. Astron. Soc. Pac., San Francisco, p. 3
Muzerolle J., Furlan E., Flaherty K., Balog Z., Gutermuth R., 2013, Nat, 493, 378
Niinuma K. et al., 2011, PASJ, 63, 9
Nordhagen S., Herbst W., Rhode K. L., Williams E. C., 2006, AJ, 132, 1555
Norris R. P., Whiteoak J. B., Caswell J. L., Wieringa M. H., Gough R. G., 1993, ApJ, 412, 222
Ott M., Witzel A., Quirrenbach A., Krichbaum T. P., Standke K. J., Schalinski C. J., Hummel C. A., 1994, A&A, 284, 331
Pestalozzi M. R., Elitzur M., Conway J. E., Booth R. S., 2004, ApJ, 603, L113
Pestalozzi M. R., Minier V., Booth R. S., 2005, A&A, 432, 737
Phillips C. J., Norris R. P., Ellingsen S. P., McCulloch P. M., 1998, MNRAS, 300, 1131
Press W. H., Rybicki G. B., 1989, ApJ, 338, 277
Sana H. et al., 2012, Sci, 337, 444
Sanna A., Reid M. J., Moscadelli L., Dame T. M., Menten K. M., Brunthaler A., Zheng X. W., Xu Y., 2009, ApJ, 706, 464
Scargle J., 1989, ApJ, 343, 874
Sobolev A. M., Cragg D. M., Godfrey P. D., 1997, A&A, 324, 211
Stellingwerf R., 1978, ApJ, 224, 953
Szymczak M., Wolak P., Bartkiewicz a., van Langevelde H. J., 2011, A&A, 531, L3
van der Walt D. J., 2011, AJ, 141, 152
van der Walt D. J., Goedhart S., Gaylard M. J., 2009, MNRAS, 398, 961
Walsh A. J., Burton M. G., Hyland A. R., Robinson G., 1998, MNRAS, 301, 640

SUPPORTING INFORMATION

Additional Supporting Information may be found in the online version of this article:

Figure S1. Lomb-Scargle periodogram for peak velocity channels in G9.62+0.19E at 6.7 GHz.
Figure S2. Lomb-Scargle periodogram for peak velocity channels in G9.62+0.19E at 12.2 GHz.
Figure S3. Lomb-Scargle periodogram for peak velocity channels in G188.95+0.89 at 6.7 GHz.
Figure S4. Lomb-Scargle periodogram for peak velocity channels in G188.95+0.89 at 12.2 GHz.
Figure S5. Lomb-Scargle periodogram for peak velocity channels in G328.24-0.55 at 6.7 GHz.
Figure S6. Lomb-Scargle periodogram for the peak velocity channel in G328.24-0.55 at 12.2 GHz.
Figure S7. Lomb-Scargle periodogram for peak velocity channels in G331.13-0.24 at 6.7 GHz.
Figure S8. Lomb-Scargle periodogram for peak velocity channels in G338.93-0.06 at 6.7 GHz.
Figure S9. Lomb-Scargle periodogram for the peak velocity channel in G338.93-0.06 at 12.2 GHz.
Figure S10. Lomb-Scargle periodogram for peak velocity channels in G339.62-0.12 at 6.7 GHz (http://mnras.oxfordjournals.org/lookup/suppl/doi:10.1093/mnras/stt2009/-/DC1).

Please note: Oxford University Press are not responsible for the content or functionality of any supporting materials supplied by the authors. Any queries (other than missing material) should be directed to the corresponding author for the article.

This paper has been typeset from a TEX/LATEX file prepared by the author.